Influence of Sr, Fe and Mn content and casting process on the microstructures and mechanical properties of AlSi7Cu3 alloy

Zaidao Li, Nathalie Limodin, Amina Tandjaoui, Philippe Quaegebeur, Pierre Osmond, David Balloy

Influence of Sr, Fe and Mn content and casting process on the microstructures and mechanical properties of AlSi7Cu3 alloy

Zaidao Li [a,c], Nathalie Limodin [a], Amina Tandjaoui [a], Philippe Quaegebeur [a], Pierre Osmond [b] David Balloy [c]

[a] Laboratoire de Mécanique de Lille (LML), FRE 3723; Ecole Centrale de Lille, 59651, Villeneuve d'Ascq, France

[b] PSA Peugeot Citröen, Direction de la Recherche et de l'Innovation Automobile, Route de Gisy-78943, Vélizy-Villacoublay Cedex, France

[c] Unité Matériaux et Transformations, UMR CNRS 8207, Univ. Lille 1, 59655, Villeneuve d'Ascq, France

Abstract: The effects of Strontium (Sr), Iron (Fe) and Manganese (Mn) additions, casting process (i.e., cooling rate) on the microstructures and mechanical properties of AlSi7Cu3 alloy were investigated. 2D and 3D metallographic and image analysis have been performed to measure the microstructural changes occurring at different Sr, Fe and Mn levels and casting process. The evolution of mechanical properties of the alloys has been monitored by Brinell and Vickers hardness measurement and tensile tests. Addition of Sr slightly refines the eutectic silicon particles but it also introduces more pores. The combined addition of Fe and Mn induces an increase of Fe-rich intermetallic compounds which include both α-$Al_{15}(Fe,Mn)_3Si_2$ and β-Al_5FeSi phase, while the volume fraction of porosity decreases with the Fe and Mn content increase. The secondary dendrite arm spacing slightly decreases with the addition of Sr, Fe and Mn alloying elements.

Keywords: casting aluminium alloys, microstructure, mechanical characterization, microanalysis, tomography

1 Introduction

Aluminum-silicon (Al-Si) system alloys are characterized by their excellent castability, high thermal conductivity and low thermal expansion coefficient [1]. These characteristics make them excellent candidates for automotive and aerospace applications.

The microstructure of alloys can be influenced by several alloying elements and casting process parameters [2]. As the alloy properties are strongly affected by the resulting microstructure, controlling and understanding the influence of microstructure is a key issue in many industries. The microstructure of Al-Si alloys is defined by the size, morphology and content of eutectic Si phase, intermetallic compounds, and pores. Understanding the complex relationship between the mechanical properties and the microstructure of the Al-Si alloy requires a reliable way to identify and quantify this microstructure.

Al-Si alloys are often used for the production of automotive parts such as cylinder heads. To manufacture such complex parts at a reduced cost, the Lost Foam Casting (LFC) process offers a promising alternative to the traditional gravity Die Casting (DC) method in permanent mold with sand cores. However, the LFC process tend to show lower mechanical properties than parts produced with conventional casting processes due to the low cooling rate [3], thus it is necessary to compare the microstructures and properties of DC and LFC alloy. In addition, the alloy composition of cylinder heads produced from secondary alloys may vary within a given composition tolerance for each element [4]. This composition tolerance introduces microstructural variations that need to be understood. The influence of different alloys elements addition on the microstructure and mechanical properties of the Al-Si alloy has been already studied by some researchers [2, 5]. Strontium (Sr) is commonly added to Al-Si alloys to improve mechanical properties by reducing the size and changing the morphology of the eutectic Si particles [6], while more dispersed and round pores will be introduced with the Sr addition [7]. In recent years, more secondary (recycled) aluminium alloys are used to replace primary alloys due to their lower energy consumption and comparable properties with primary aluminium alloys [8]. Iron (Fe) is one of the most undesirable impurities in recycled aluminium alloys due to the formation of brittle intermetallics, called plate-like β-Al_5FeSi intermetallics, which have been shown to act as stress raisers and lead to crack initiation and are thus detrimental to in-service mechanical properties [9, 10]. The surface fraction and size of Fe-intermetallics in Al-Si alloy is affected by the Fe level [11] and cooling rate [12]. The addition of manganese (Mn) can change the morphology of iron intermetallics from the deleterious plate-like morphology of the β-Al_5FeSi phase to the less harmful Chinese script morphology of the α-$Al_{15}(Fe,Mn)_3Si_2$ phase, and the degree of transformation depends on the cooling rate [12]. Seifeddine et al. [13] showed that Mn additions are not able to totally nullify the formation of β-Al_5FeSi-needles onto α-$Al_{15}(Fe,Mn)_3Si_2$-Chinese scripts at high cooling rates for a 2:1 Mn:Fe ratio in an Al-9w.%Si alloy. In addition, several researchers have also investigated the effect of Fe on the porosity formation in Al-Si cast alloys [14-16]. Moustafa [17] reported that a high Fe content can promote the formation of pores because the precipitation of β-phase can prevent the liquid metal to fill the spaces between the branched platelets as β-phase can block the interdendritic liquid channels and thus hinder liquid flow and feeding during solidification. Dinnis et al. [18] reported that the effect of Fe content on porosity depends apparently on both the Si and copper (Cu) content. Another study by Taylor et al. [16] indicates that a minimum level of porosity exists at an intermediate Fe content.

However, most of this research has been based on two-dimensional (2D) analysis of the microstructure due to the complexity in generating or accurately representing their three-dimensional (3D) microstructure. In fact, the over-idealized 2D microstructure does not effectively allow understanding the relationship between the microstructure and mechanical behavior of the alloys, especially for the pores, which play a vital role in determining the mechanical behavior [19].Thus, a preliminary 3D characterization of the pores to study how they are affected by alloy elements and casting process would appear to be particularly important.

In the present investigation, a full metallographic 2D and 3D characterization of the microstructure through optical- and Scanning Electron Microscopy (SEM) and laboratory X-ray tomography was performed in order to study the influence of variation in Sr, Fe, and Mn content within the composition tolerance of the AlSi7Cu3 alloy and of the casting process, i.e. Die casting (DC) and Lost Foam Casting (LFC), on the microstructure. The relationship between microstructure and mechanical properties was also studied. In order to achieve this, two primary, i.e. with low Fe levels, DC AlSi7Cu3 alloys with a different Sr content were used to study the Sr effect on the microstructure and mechanical properties. At the same time, two secondary, i.e. with high Fe levels, DC AlSi7Cu3 alloys with different Mn:Fe ratios were used to clarify the role of Fe and Mn. Besides, the secondary alloy with a lower ratio of Mn

to Fe, which is usually used to manufacture commercial cylinder heads, was produced by two different casting methods, i.e. DC vs LFC, in order to study the effect of these processes.

2 Experimental procedures

2.1 Alloys and casting procedure

For the two primary DC AlSi7Cu3 alloys with different Sr content (i.e. alloy A and B), the base alloys were supplied as commercial ingots of primary alloy. Sr addition was achieved by introducing different amounts of an Al–10 wt. % Sr master alloy to the molten base alloy. For the two DC AlSi7Cu3 alloys with different Mn:Fe ratios (i.e. alloy C and D), the base alloy was received as ingots of secondary alloy. Different amounts of Sr, Fe and Mn in the form of Al–10 wt. % Sr, Al–25%Fe and Al–25%Mn master alloys were added into the melt, the holding time was over 60 min in the electric resistance furnace to achieve homogeneous melts.

The ingots were cut into smaller pieces, dried, and melted in a silicon carbide crucible, using an electric resistance furnace (temperature deviation of ±5 °C). The melting temperature was held at 735 ± 5 °C. High purity dry argon was used as degasser; the degassing period was 12min with a flow of 2l/min. The melt was then poured into the mold at about 720 ℃.

After the casting, 30 cylindrical cast specimens with the 20 mm diameter and 200 mm length were obtained for each composition, and each specimen was examined with X-ray radiography in order to assess the specimen porosity level. Each specimen was classified with a range between 1 to 8 according to the ASTM E155 standard [20]. The compositions of the experimental alloys were measured using a mass spectrometer and the results are given in Table 1. Some specimens that have a chemical composition, given in Table 1, similar to DC alloy C were cut from industrially manufactured cylinder heads obtained by LFC process.

Table 1 Chemical compositions of the experimental AlSi7Cu3 alloys (wt. %)

Alloy	Casting method	Al	Si	Fe	Mn	Mn/Fe	Sr	Cu	Mg	Ti	Pb	Zn
A	DC	bal.	6.91	0.10	0.007	0.07	**0.0047**	2.89	0.29	0.11	0.003	0.022
B	DC	bal.	7.01	0.14	0.010	**0.07**	**0.0133**	3.36	0.30	0.11	0.004	0.033
C	DC	bal.	7.66	**0.49**	**0.130**	**0.26**	0.0120	3.67	0.31	0.11	0.054	0.33
	LFC	bal.	7.85	**0.30**	**0.190**	0.63	0.0120	3.05	0.28	0.098	0.015	0.16
D	DC	bal.	7.00	**0.80**	**0.510**	**0.64**	0.0100	3.45	0.28	0.12	0.05	0.24

2.2 Microstructural and mechanical characterization

The specimens for the characterization of the microstructure and mechanical properties were extracted from the center of cylindrical parts.

2.2.1 Characterization technologies

The measurement of pores characteristics was performed with X-ray laboratory Computed Tomography (Lab-CT) at a 2.75×2.75×2.75 μm^3 voxel size. Thanks to the absorption contrast provided by Lab-CT, the pores can be easily distinguished from the matrix. X-ray microtomography was realized at the LML laboratory (Lille, France) within an Ultratom (RX Solution) Lab-CT system fitted with a Nanofocus tube at an acceleration voltage of 70 kV. The specimen was placed on a rotating stage in the tomography chamber between the X-ray source and a Flat panel detector of dimensions 1920×1496 voxels. A set of 4320 radiographs (scan) were taken while the sample was rotating over 360° along its vertical axis. With an acquisition time per image of 330 ms, one scan lasted about 2 hours. The average analyzed volume for each alloy was about 32 mm^3.

3D characterization for the Si phase could not be achieved with Lab-CT as Al and Si have close atomic numbers hence similar X-ray attenuation. As for intermetallic compounds, their size in DC alloys is too small compared to the tomography resolution. However, optical microscopy at a pixel size of 0.7µm gives enough contrast between the intermetallic phase, eutectic silicon and Al matrix, thus 2D metallographic analysis was used to characterize the Si phase and intermetallic compounds. The 2D microstructure observations were done using a Nikon YM-EPI light microscope equipped with a Sony color video camera and a JEOL 7800 F LV SEM. The EDS analyses were performed using the equipped OXFORD System Aztec and an X-Max 80 mm^2 premium spectrometer Microanalysis System. The size and morphology of eutectic silicon phase and intermetallic compounds were estimated for each alloy on polished samples covering an average area of about 1.2 mm^2 large enough to be representative of the whole sample.

2.2.2 Image processing

2D and 3D images were processed and analyzed using ImageJ/Fiji and Avizo Fire softwares, respectively, using the following procedure: (i) median filtering was applied prior to segmentation in order to reduce the noise in the image, (ii) a simple grayscale thresholding technique was used to segment the different phases, i.e. hard inclusions in the 2D images and pores in the 3D images. Quantitative analysis could then be realized to label the objects, i.e. to attribute each individual object a given label or color, and to measure several characteristics of the labelled objects. Objects that are small as compared to the resolution of the images, i.e. with a volume less than 9 voxels in 3D or with an area less than 9 pixels in 2D, were neglected and discarded from the analysis.

The main parameters used to characterize the morphology of intermetallics, Si particles and pores are Feret diameter and sphericity (F). Feret diameter is defined as the longest distance measured between two parallel tangents on each side of the 2D or 3D object of interest. Feret diameter was used to assess the size of either pores or hard inclusions as it could better reflect not only the size but also the shape of objects. Sphericity corresponds to the ratio between the particle area and the area of the circle with the same perimeter as the object in 2D [21] or to the ratio between the object volume and the volume of a sphere with the same surface as the object in 3D.

In order to determine the average value of the Secondary Dendrite Arm Spacing (SDAS) in one sample, the size of SDAS was obtained as an average value of at least 10 measurements.

2.2.3 Mechanical testing

Hardness measurements were performed on the polished samples. Vickers hardness measurements were carried out using a load of 30 kg and a 15 second dwell time. Each measurement represents the average of at least twelve indentation readings taken from different areas of the specimen.

Tensile tests were conducted as per ISO 6892-1 [22] on dog-bone shaped round samples of 5 mm gauge diameter and 30 mm gauge length. For each alloy, three tensile tests were carried out on a computer controlled testing machine (Instron) at a constant cross head speed of 1 mm/min. All the tests were performed at ambient temperature (~25 °C). A strain gauge extensometer (gauge length of 25 mm) was used to measure the 0.2% proof stress, ultimate tensile strength and the elongation up to fracture.

3 Results and discussion

3.1 Microstructure examination

3.1.1 Secondary Dendrite Arm Spacing (SDAS) analysis

The typical microstructures obtained from alloy C in the cross section of samples are shown in Figure 1; the micrographs (a) and (b) refer to the DC and LFC, respectively. Compared with the DC alloy, the LFC alloy shows a coarser microstructure, i.e. larger SDAS, platelet eutectic Si particles, needle-like iron-intermetallics; SDAS values are given in Table 2. The average size of SDAS increased from 18.4µm to 76.4µm when the cooling rate decreased from 30°C/s (DC) to 0.8°C/s (LFC) [23].

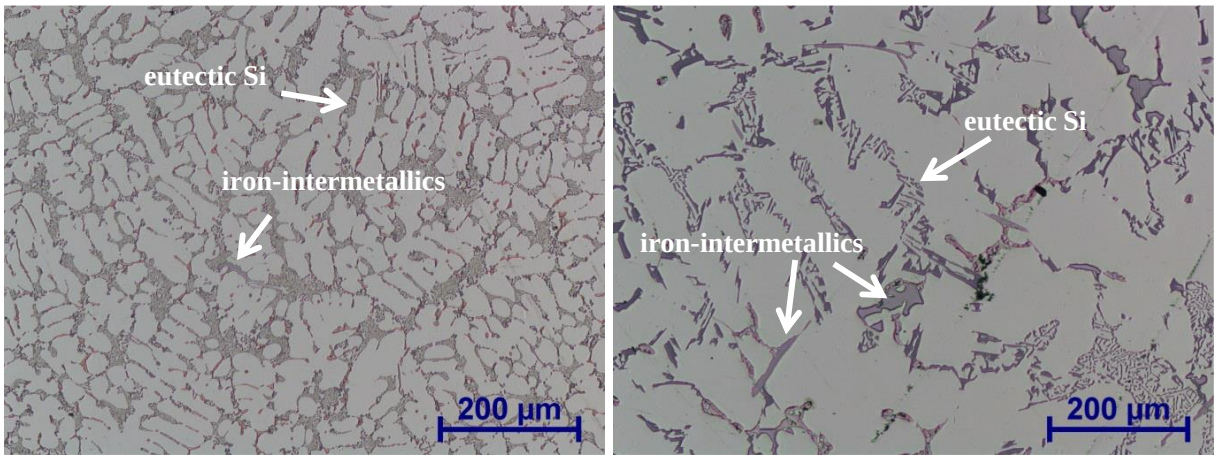

Figure 1 Optical microstructures of Alloy C in (a) DC and (b) LFC

Although the size of the dendrites appears strongly affected by the cooling rate, the chemical composition of the alloy has also some effect on this structural characteristic.

In order to study the effect of Sr, Fe and Mn content on the size of the microstructure, SDAS measurements were performed on the four different alloys having the chemical composition shown in Table 1. The average SDAS values are listed in Table 2. Comparing alloy A and alloy B, the addition of Sr from 47ppm to 133ppm leads to a SDAS reduction of about 6.25%, besides the SDAS slightly decreased from 19.5 µm to 17.0 µm when the content of Fe and Mn increased from 0.14 wt. % and 0.01 wt. % to 0.8 wt. % and 0.51 wt. %, respectively **(**Table 2**)**.

SDAS variation appears slightly connected to the initial chemical composition of the alloy, i.e. to the Sr, Fe and Mn content. Similar results from Sanna et al. [24] and Fabrizi et al. [5] confirmed that SDAS varies when the content of alloying elements such as Sr, Cu, Fe and Mg is changed in Al-Si-Cu based DC alloys for a fixed solidification time. The refining effect of alloying elements on SDAS may be attributable to the solute segregation limiting the effective diffusion length when the dendrites are first formed during the solidification [25]; a higher concentration of alloying elements will cause the precipitation of finer dendrites and vice versa.

Table 2 SDAS in four different studied alloys

Alloy code	Casting method	SDAS (µm) Mean	SDAS (µm) Standard deviation
A	DC	20.8	2.4
B	DC	19.5	2.4
C	DC	18.4	2.1
	LFC	76.4	6.9
D	DC	17.0	2.3

3.1.2 Porosity characterization

To the authors' knowledge, no experimental results have been reported showing use of 3D characterization of pores to study the influence of chemical composition on microstructure of Al-Si alloy. Some researchers [7, 18] have studied the influence of different elements on pore formation for Al-Si alloys. However, their measurements are based on 2D analysis which cannot accurately characterize the features of pore. In the present work, in order to quantitatively characterize the distribution and size of the pores in 3D, cylindrical specimens with 3 mm length and 4 mm diameter were extracted from the center of the cast cylindrical bars and scanned with X-ray tomography. This allowed determining the volume fraction and characteristics of pores. Figure 2 shows the 3D rendering of the pores in different alloys and for different casting process at a voxel size of 2.45 µm. The measured pores characteristics for the four different AlSi7Cu3 alloys are provided in Table 3.

Table 3 Porosity characteristics as a function of alloy composition and casting method.

Alloy	Casting method	Volume fraction %	Feret diameter (µm) Av.	Feret diameter (µm) Max.	Analysed volume (mm^3)	Density (particles/mm^3)
A	DC	0.034	30	276	30.8	94
B	DC	0.065	28	294	31.2	200
C	DC	0.045	27	279	31.2	174
	LFC	0.940	64	1536	33.0	17
D	DC	0.032	24	299	31.6	97

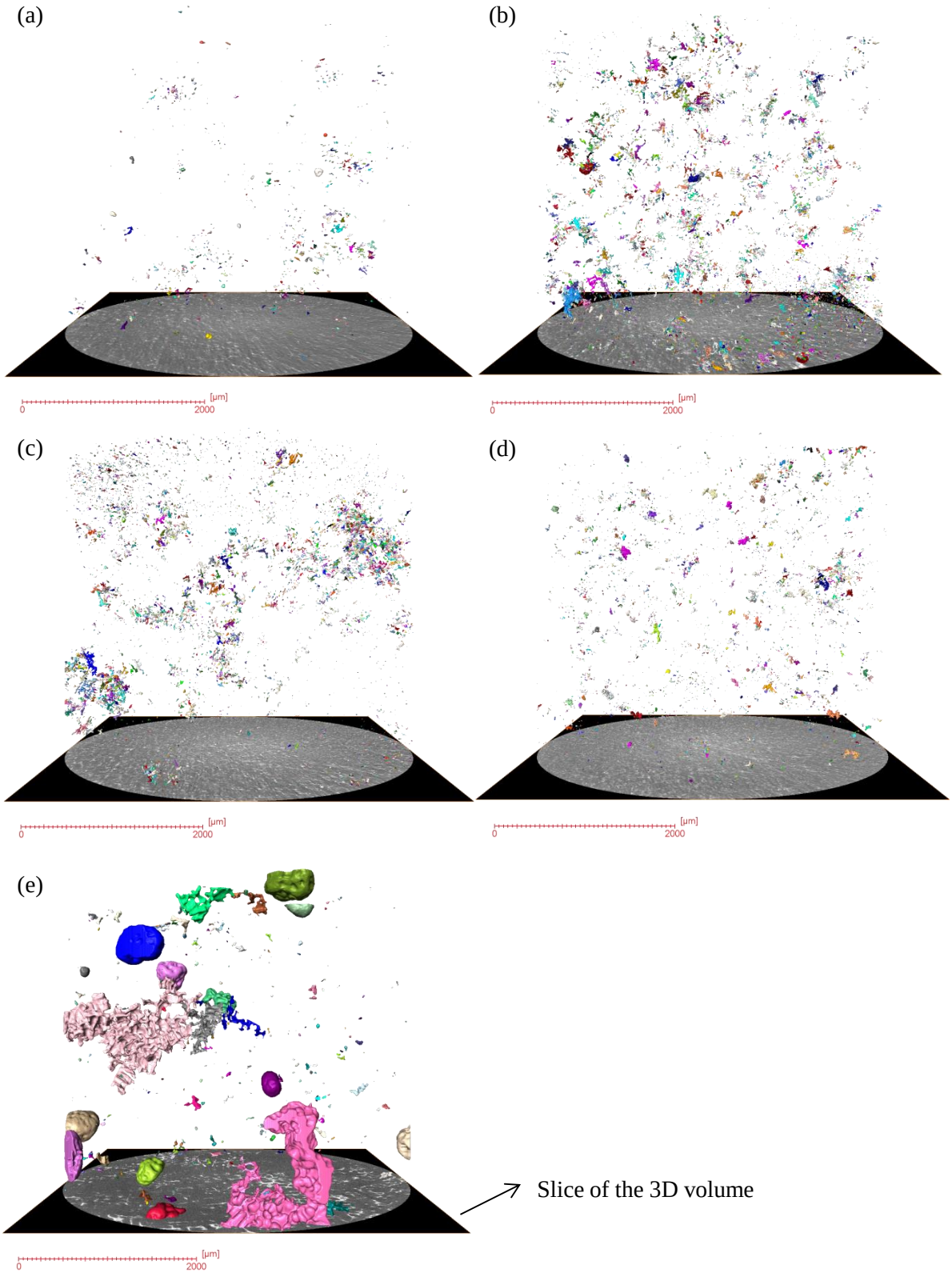

Figure 2 3D rendering of pores for alloys (a) A, (b) B, (c) C and (d) D in DC, and (e) alloy C in LFC. (Dimension: Ø3.7mm×Height 3mm)

In alloys A and B, the number and the volume fraction of pores increased by more than twice (Table 3) with the Sr content increase from 47ppm to 133ppm (see Table 1). The distributions of pores as a function of Feret diameter in alloy A and B in Figure 3 show that increasing Sr content introduces more fine pores in the range of 10 to 50 µm but also more large microshrinkage cavities in the range of 50 to 300 µm. The addition of Sr changes the amount of porosity as already reported by several studies [7, 26, 27] due to a complex interaction of different parameters. Liu et al. [27] explain the increased porosity level with the content of Sr by the formation of strontium oxides due to the high affinity of Sr for oxygen; these strontium oxides are frequently observed associated with microporosity in Sr-modified alloys. Emadi et al. [21] reported that the addition of Sr can reduce the surface tension, an effect that can facilitate porosity formation and results in increased porosity. Argo and Gruzleski [28] indicate that interdendritic feeding becomes more difficult in modified alloys as they have a longer mushy zone due to the depression of the eutectic temperature. Consequently, more pores may form over a longer period, which explains the larger microshrinkage cavities observed in alloy B.

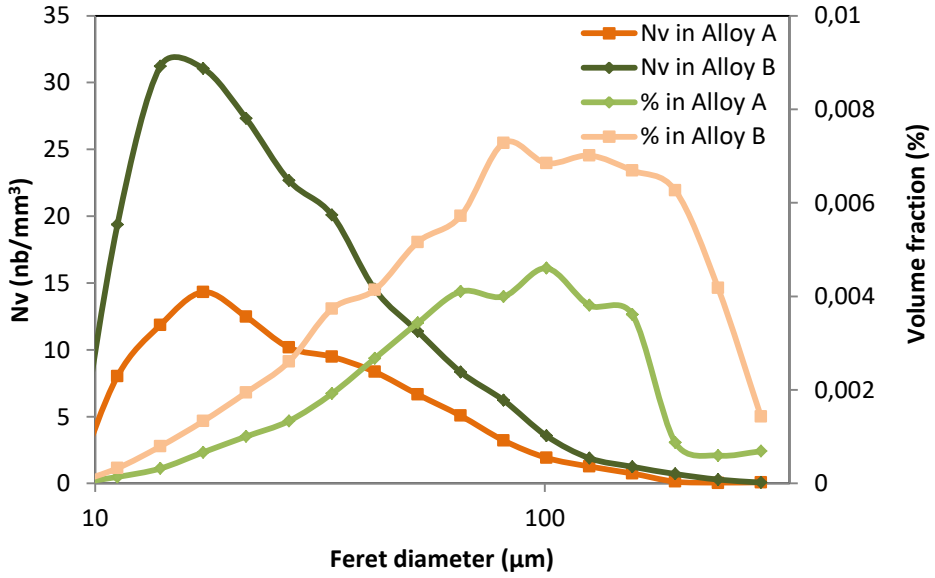

Figure 3 Size distribution of pores in number (Nv) and in volume (%) for alloy A and B in Die casting

Prior to 3D characterization of pores in DC alloys, the presence of porosity was studied by X-ray radiography for DC alloys B, C and D; for each alloy, 30 specimens were analyzed. ASTM E155 standard gives the criteria to define the 'qualitative' amount of porosity allowable and defines 8 defect classes. Figure 4 shows the frequency distribution of shrinkage cavity level according to the standard ASTM E155. The maximum pore density is observed at alloy B which has the lowest Fe and Mn content among the four alloys. The result of 2D X-ray radiography characterization shows that the porosity level seems to decrease with an increase in the Fe and Mn content.

From the 3D characterization results, the volume fraction of pores decreased from 0.065% to 0.032% when the Fe and Mn content increased from 0.14% and 0.01% to 0.80% and 0.51% for the DC alloys B, C and D (Table 2). This confirmed the previous qualitative results of 2D characterization for pores, and it also proves that decreased porosity level results from an increase of Fe and Mn content in some extent. However, this result is in contradiction with some reports [14, 29] that claim iron-intermetallics

help nucleate pores. Studies made by Taylor et al. [16] and Dinnis et al. [18] indicates that the existence of a critical Fe content for a minimum porosity formation in unmodified Al-Si-Cu alloy, and that different solidification paths resulting from different Fe levels lead to variations in microstructural permeability, i.e. interdendritic feedability, and hence in porosity formation. Besides in the study of Puncreobutr et al. [30], larger pores were observed to nucleate before the intermetallics during in-situ solidification of an A319 alloy at 0.36°C/s. Thus, maybe it is more interesting to study the influence of Fe content on the porosity formation through in-situ solidification experiment.

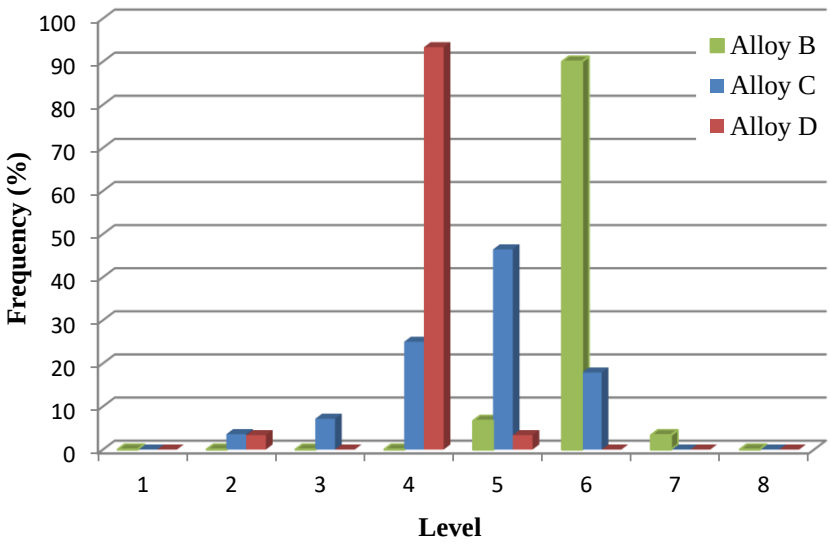

Figure 4 The frequency distribution of shrinkage cavity level according to the standard ASTM E155 for alloys B, C and D

In the present work, the decrease in porosity content could also be due to the increase of Mn content in alloys B, C and D. As reported by Dinnis et al. [31], the addition of Mn also can reduce the amount of porosity, because Mn additions reduce the poisoning of Al-Si eutectic nucleation sites by Fe. This leads to the formation of a greater number of smaller Al-Si grains during solidification and in turn results in improved permeability and feeding, and hence a reduction in porosity. According to Dinnis et al. [31], the addition of 0.5%Mn to a 1%Fe-containing Al-9%Si alloy can reduce porosity levels to those obtained in the same alloy with 0.6%Fe (i.e. the critical iron content for that composition). Moreover, as mentioned before, the decrease of Sr content from 130 ppm to 100 ppm also can contribute to the slight decrease of porosity fraction for alloy B, C and D. These may be the reasons why alloy D, which has higher Fe/Mn content and lower Sr content, has lower porosity level.

The effect of casting process (DC vs. LFC) on the porosity was also investigated. As shown in Figure 2, a decrease in cooling rate from 30°C/s (DC) to 0.8°C/s (LFC) increases both the total volume of porosity and the average pore size measured in alloy C (Table 3).

The distribution of pores as function of Feret diameter for DC and LFC is shown in Figure 5. DC alloy has more micropores within the range of 10 to 200 µm than LFC alloy. However LFC alloy has larger pores with a maximum Feret diameter up to 1535µm, and the largest pore represent approximately 45% of the total volume fraction of the pores population (see Figure 5). The significant difference in porosity content and size between DC and LFC alloys can be explained by the different cooling rate during solidification. At increasing solidification rates, hydrogen has less time to diffuse into the interdendritic spaces of the partially solidified metal [2], resulting in more finely dispersed porosity. Furthermore, the

higher temperature gradients present at higher solidification rates tend to limit the length of the mushy zone, making feeding easier and retarding porosity formation [32]. In addition, LFC casting method utilizes an evaporative pattern which may increase the entrapped gas content in the alloy and hence lead to increased porosity. The spherical gas porosity, which is observed in LFC alloy (Figure 2(e)), could be due to entrapment of gas bubbles in the casting [33].

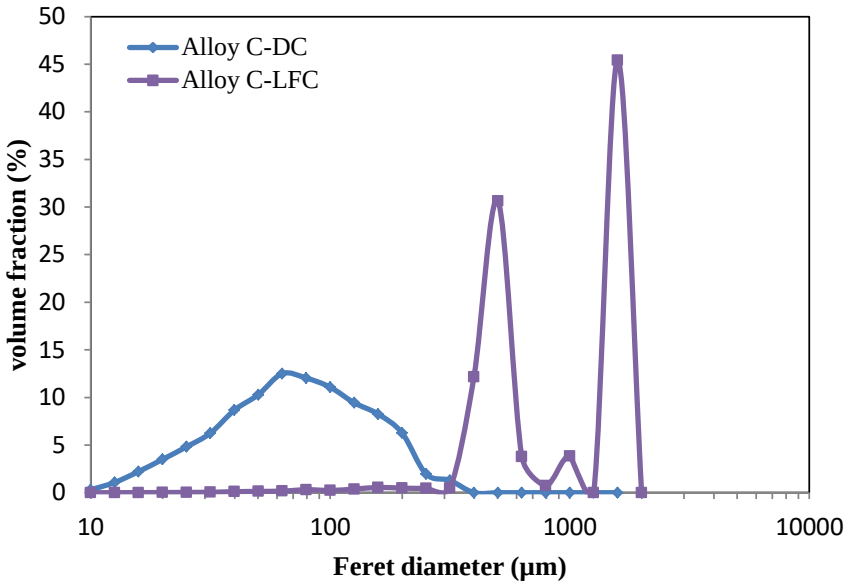

Figure 5 The distribution of pores as function of Feret diameter for DC and LFC alloys

3.1.3 Eutectic Si characterization

Mechanical properties of Al–Si alloys are known to be influenced by the size, shape and distribution of eutectic silicon present in the microstructure. Thus, Al-Si alloys are generally subjected to Si modification in order to improve mechanical properties. Si modification, which transforms the acicular silicon morphology to fibrous one resulting in a noticeable improvement in elongation and strength [34], can be achieved in three different ways: modification by addition of some elements (chemical modification) or with a rapid cooling rate (quench modification), globalization by high temperature annealing.

3.1.3.1 The effect of Sr content

The effect of Sr as a modifying agent on the microstructure of gravity die cast Al–Si alloys is widely reported in literature [6, 35, 36]. The addition of Sr promotes the formation of a fibrous silicon structure by retarding the growth rate of silicon [34]. The effect of Sr content on the modification of the eutectic Si particles was studied in alloys A and B. The micrographs of alloy A (Figure 6a) and alloy B (Figure 6b) in different magnification are compared in Figure 6**:** eutectic Si appears as the darkest phase. In both cases the effect of modification of eutectic Si is visible. However, significant differences in the extent of the modification between alloy A and B cannot be observed by naked eye from Figure 6 . Thus, quantitative metallographic characterization of eutectic Si particles was performed with image analysis in terms of sphericity. The distributions of eutectic Si particles morphology in Figure 8 show that more eutectic Si particles with sphericity above 0.4 were present in alloy B compared to alloy A; this means that the amount of plate-like morphology eutectic Si decreased with an increase in the content of Sr. As a result, the higher the Sr content, the more eutectic Si shows a fibrous and globular morphology in Sr-modified alloy.

Eutectic Si particles modification was shown to depend not only on the cooling rate, but also on the Sr content. Besides the effect due to cooling rate is stronger than that due to Sr addition at high cooling rate (SDAS=20µm).

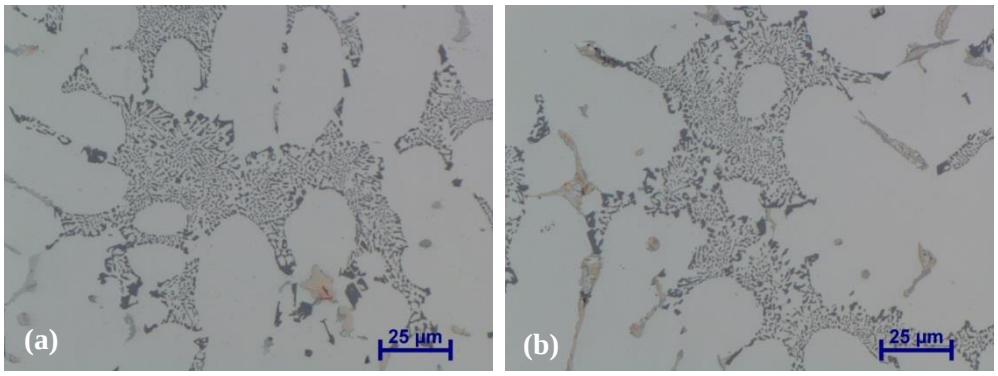

Figure 6 Optical micrographs of alloy A (a) and alloy B (b) in Permanent mold casting; eutectic Si is the dark phase

3.1.3.2 The effect of cooling rate

A typical eutectic microstructure of both DC and LFC AlSi7Cu3 alloy is shown in Figure 7 in the same magnification. From this figure, casting process appears to have a significant impact on eutectic modification for AlSi7Cu3 alloy. The DC alloy in Figure 6(a) clearly shows the fine fibrous morphology of the eutectic Si phase. In contrast, the LFC alloy in Figure 7(b) reveals the eutectic Si phase that appears as platelets.

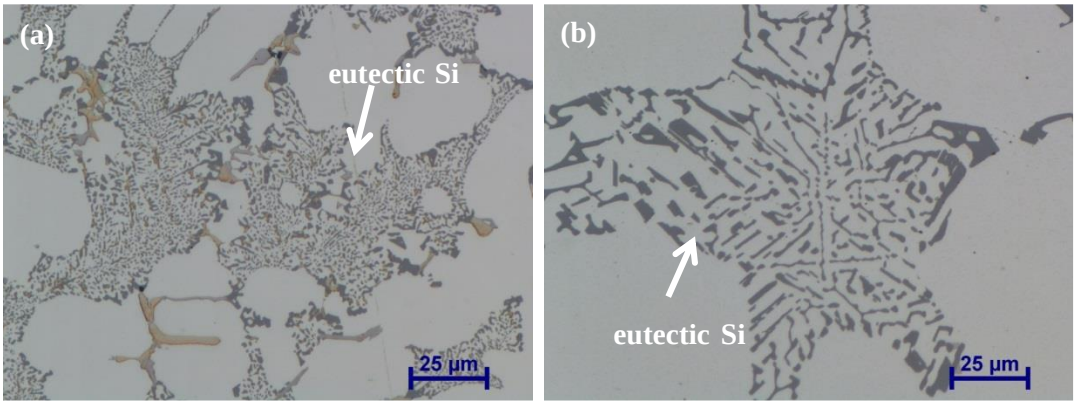

Figure 7 Optical micrographs showing eutectic Si microstructure in (a) Permanent mold casting, (b) Lost Foam casting for alloy C

The distributions of eutectic Si phase as function of the Feret diameter in DC and LFC alloy C are shown in Figure 8a. Due to the differences in the cooling rate between LFC and DC, the distributions of eutectic Si phase as function of the Feret diameter are quite different from each other. More small eutectic Si particles, i.e. with a size between 1 and 13 µm, are distributed in DC alloy compared to LFC alloy. On the other hand, more large eutectic Si particles, which correspond to most of the surface fraction, were revealed in LFC alloy; the largest Feret diameter of eutectic Si can reach up to 141µm in LFC compared to 32µm in DC. In addition, the distributions of sphericity in Figure 8b show that at low cooling rate (i.e. LFC alloy), the alloy C shows more Si particles with sphericity less than 0.3 than at high cooling rate (i.e. DC alloy). As shown in Figure 6, most of the eutectic Si present in DC appears with a fibrous morphology when the Sr content is 120 ppm in alloy C. However, the addition of the same Sr level to

LFC AlSi7Cu3 alloy was less effective in modifying the morphology of eutectic Si from acicular shapes to fibrous one at low cooling rate.

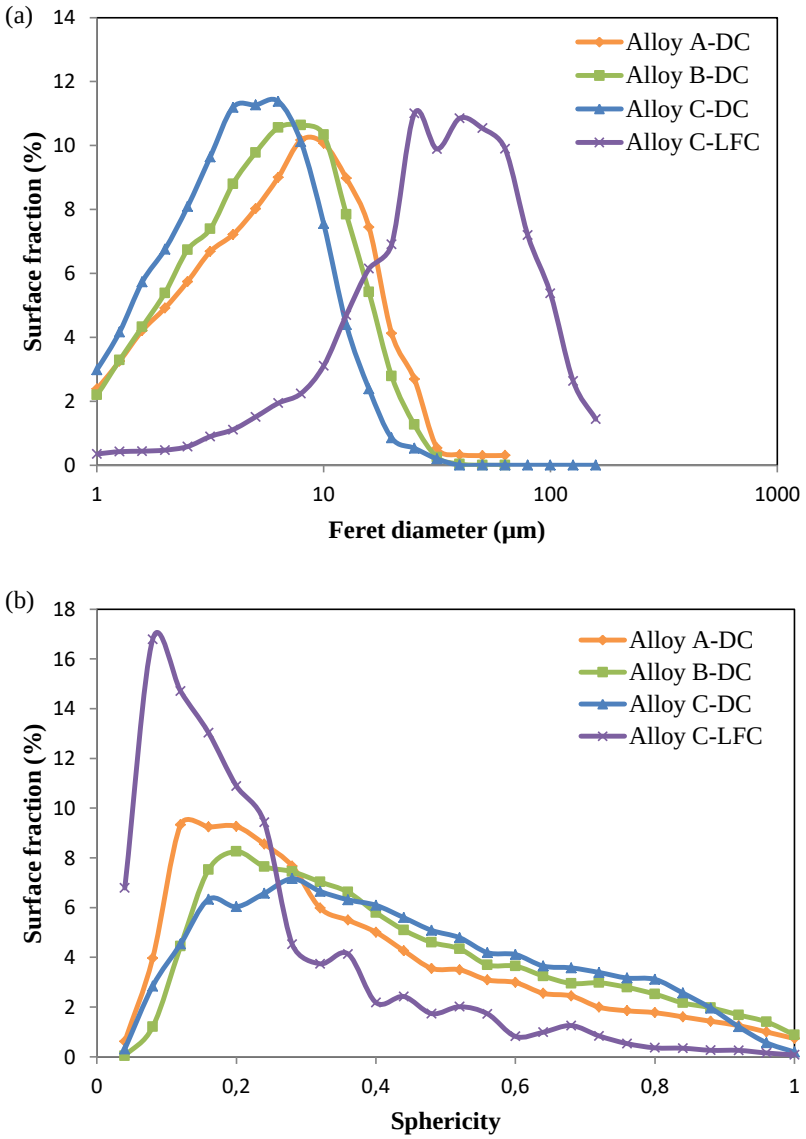

Figure 8 Distributions of Feret diameter (a) and sphericity (b) of eutectic Si particles in alloy A, B, C and D

3.1.4 Iron Intermetallic compounds

The effect of Fe, Mn content and casting process on the formation of the Fe-rich intermetallic compounds was studied in alloys B, C, and D. Manganese is often added in Al-Si alloy to alter the shape of iron intermetallics from sharp needle β-phase Al_5FeSi to a more compact type α-phase $Al_{15}(Fe,Mn)_3Si_2$ in order to reduce the embrittlement due to the needle morphology. Besides, the amount of α-phase and β-phase depends on Fe–Mn levels and on the cooling rate [2, 12].

The size and morphology, i.e. maximum length, surface area fraction, of iron-intermetallics are listed in Table 4. Small size α-phase is extremely difficult to distinguish from β-phase as their shape and gray level are similar in 2D optical images as well as in BSE images. Thus the iron-intermetallics mentioned in this part include both α- and β-phase. Figure 9a-h shows SEM micrographs of AlSi7Cu3 alloys containing different Fe and Mn content, i.e. alloy B, C and D. The composition of the iron-intermetallic

phases were measured by EDX (at%), and the results are provided in Table 5, which allowed identifying the α-phase (yellow arrow) with a script morphology (point 2 and 5) and β-phase (red arrow) with an acicular or plate-like morphology (point 1, 3 and 4) in Figure 9a-h. The distributions of iron-intermetallics as functions of Feret diameter and sphericity for alloy B, C and D are presented in Figure 10a and b. As can be seen from Figure 10a, the peak which corresponds to an average size of iron-intermetallics shifted with the Fe and Mn content changed, when the Fe and Mn content increased from 0.14% and 0.01% to 0.80% and 0.51%, the average size of iron-intermetallics increased from 5.6 μm to 15.8 μm. Figure 10b shows those iron-intermetallics with sphericity less than 0.3 increases with increasing content of Fe and Mn. It can be concluded that the amount of β-Al5FeSi phase in needle-like shape increases with the Fe content increases in the alloys.

As shown in Table 4, the maximum length and the surface fraction of the iron-intermetallics increased as the iron and manganese content increased. All alloys exhibit almost linear relationships: the higher the iron and manganese content, the higher the surface fraction of the iron-intermetallics. As seen from Figure 9c, g and h, alloy D, with the highest content of Fe and Mn, showed the largest surface fraction of iron-intermetallic compounds, which mainly consisted in the β-phase, with the needle-like morphology (Figure 9g), and in some α-phase (Figure 9h). Figure 9a and d showed that in alloy B, with the lowest content of Fe and Mn, only a few amount of small size β-Al_5FeSi phase with its typical needle-like morphology was observed. A higher fraction of iron-intermetallic compounds was detected in alloy C, with intermediate Fe content and a Mn to Fe ratio of 0.26, as compared to alloy B. Besides the addition of Mn promotes the formation of script α-phase $Al_{15}(Fe,Mn)_3Si_2$ (Figure 9b, e and f) [37]. Figure 9a, b and c show that the ratio of α and β phases increased as the Mn/Fe ratio increased from alloy B to alloy D.

Table 4 The maximum length and surface area fraction of iron-intermetallics for the alloys B to D.

Sample code	Fe wt.%	Mn wt.%	Mn/Fe	Casting process	Dimension and quantity of iron-intermetallics	
					maximum length (μm)	Surface area fraction(%)
Alloy B	0.14	0.01	0.07	DC	23.2	0.22
Alloy C	0.49	0.13	0.26	DC	56.3	1.81
	0.30	0.19	0.63	LFC	245.5	2.32
Alloy D	0.80	0.51	0.64	DC	63.0	2.48

The influence of the cooling rate on distributions of iron-intermetallics as functions of Feret diameter and sphericity can be observed in Figure 10a and b. Optical micrographs show the β platelets (arrowed) in the microstructure of alloy C in both die (Figure 11a) and lost foam casting (Figure 11b). It should be noted that the variation in size of the Fe-intermetallics in both DC and LFC alloy may also exist due to their formation at different stages during solidification. For the LFC alloy C, large size intermetallics (i.e. Feret diameter larger than 50μm) with small sphericity represent most of the total volume fraction of the intermetallics phase (Figure 10). The maximum length of iron-intermetallic compounds increased from 56.3μm to 245.5μm when the cooling rate decreases from 30°C/s (DC) to 0.8°C/s (LFC), respectively (Table 4). The longer time available for growth of iron-intermetallic at lower cooling rate may explain the larger size of intermetallics. As reported by Ceschini et al. [38], the size of intermetallic compounds mainly depends on the solidification time (i.e., cooling rate). Moreover, as reported in Table 4, the surface area fraction of the iron-intermetallics also increased from 1.81% in DC alloy to 2.32% in LFC alloy.

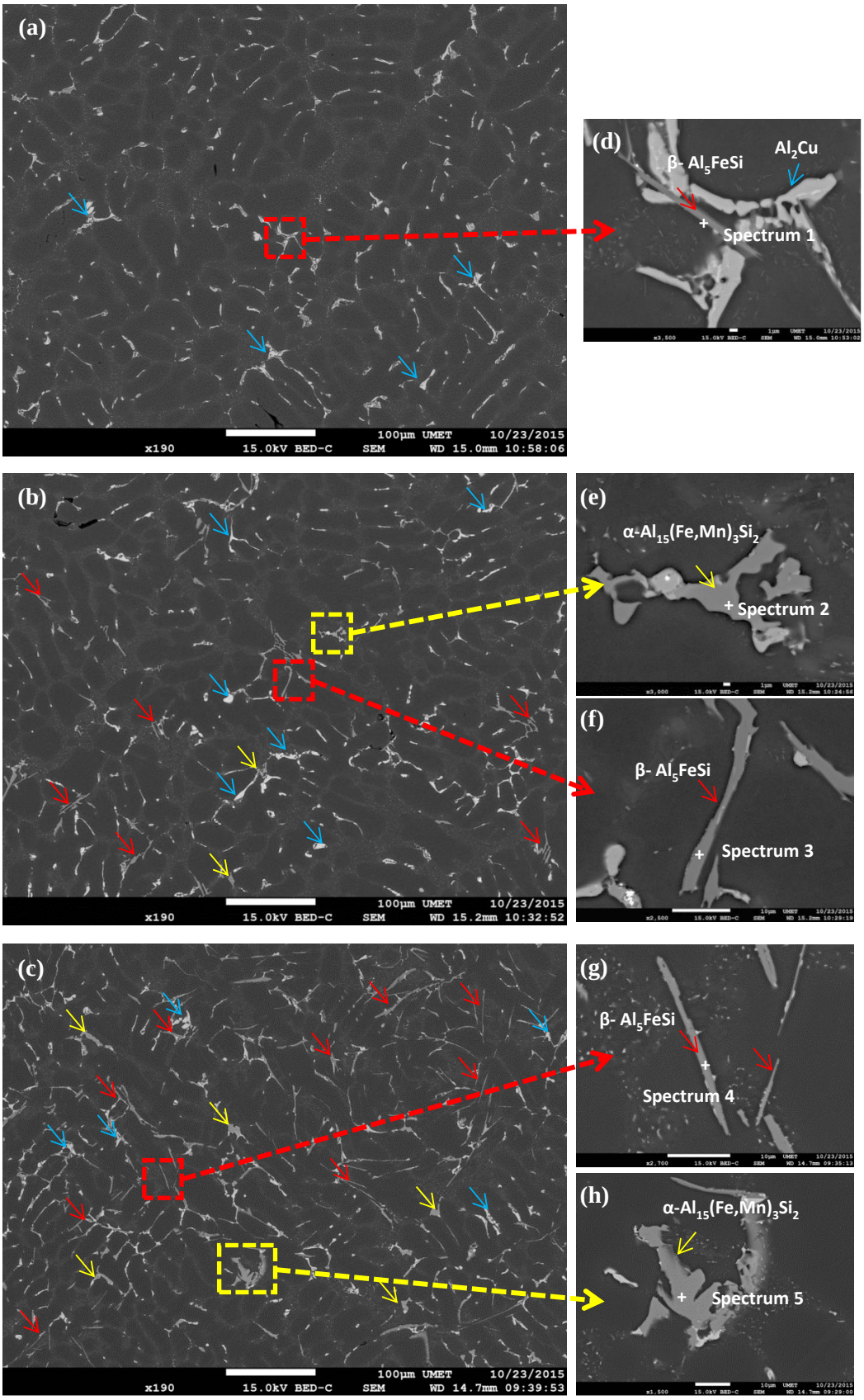

Figure 9 Backscattered electrons SEM micrographs showing the distribution of α-phase $Al_{15}(Fe,Mn)_3Si_2$ (yellow arrow) with a script morphology, β-phase Al_5FeSi (red arrow) with a needle morphology and Al_2Cu phase (blue arrow) in the (a) alloy B, (b) C and (c) D. Points of EDX microanalysis are labeled, and the results are available in Table 5.

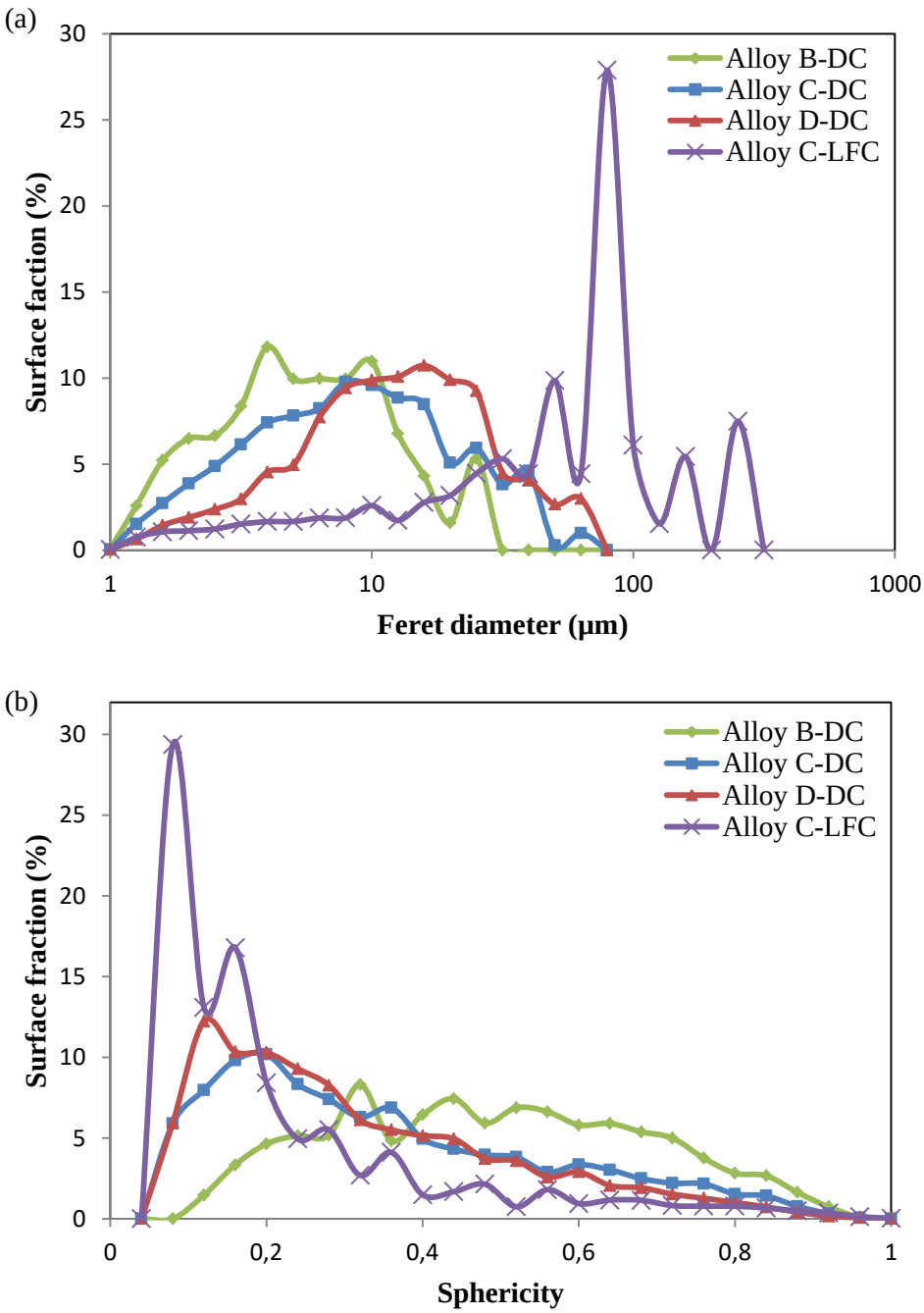

Figure 10 Distributions of iron-intermetallics as functions of Feret diameter (a) and sphericity (b) in alloy B, C and D

Table 5 EDX analysis of the intermetallic compounds in Figure 9

Alloy	Number	Element content (at. %)				Identified phase
		Al	Si	Mn	Fe	
B	1	62.97	24.76	0.34	11.93	Al_5FeSi
C	2	71.12	12.40	3.51	12.97	Al_{15} $(Fe,Mn)_3Si_2$
	3	52.59	32.49	2.56	12.36	Al_5FeSi
D	4	60.90	26.03	4.06	9.02	Al_5FeSi
	5	71.52	11.86	6.93	9.69	Al_{15} $(Fe,Mn)_3Si_2$

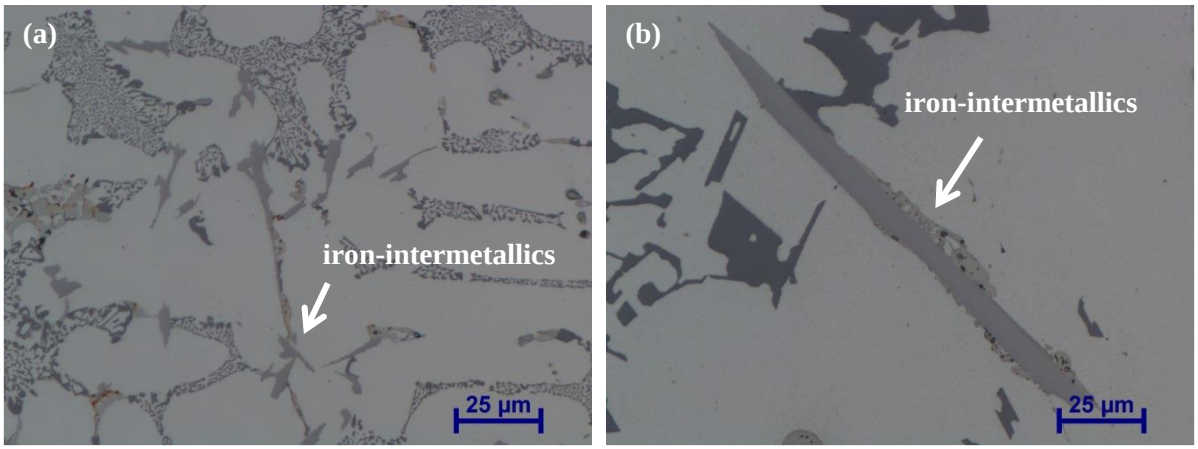

Figure 11 Optical micrographs showing iron-intermetallics in (a) Permanent mold casting, (b) Lost Foam Casting for alloy C

3.1.5 Copper based phase

Cu-bearing particles were also detected in the studied alloys. As shown in Figure 9**d**, the Al_2Cu phase connects with the iron intermetallics so that it can be reasonably assumed that the β-platelets act as nucleation sites for the copper phase particles [39].

In this work, the quantitative metallography analysis shows that alloying elements (such as Sr, Fe and Mn) have no effect of the amount and morphology of Al_2Cu phase. However, the cooling rate resulting from different casting process can significantly affect the formation of Al_2Cu phase. The distributions of Al_2Cu as functions of Feret diameter and sphericity in DC and LFC for alloy C are reported in Figure 12a and b. The LFC alloy with the lower cooling rate presents larger Al_2Cu particles, which correspond to most of the surface fraction (Figure 12**a**), this could also be attributed to the longer time available for growth of Al_2Cu phase at lower cooling rate. Figure 12**b** shows that more Al_2Cu phase with sphericity above 0.3 was present in DC alloy compared to LFC alloy. Thus, the morphology of Al_2Cu phase becomes more round with an increase in the cooling rate; this can be explained by the fact that at increasing cooling rate, an increased nuclei number could affect the number, and thus, the size and morphology of the Al_2Cu phase precipitates [40].

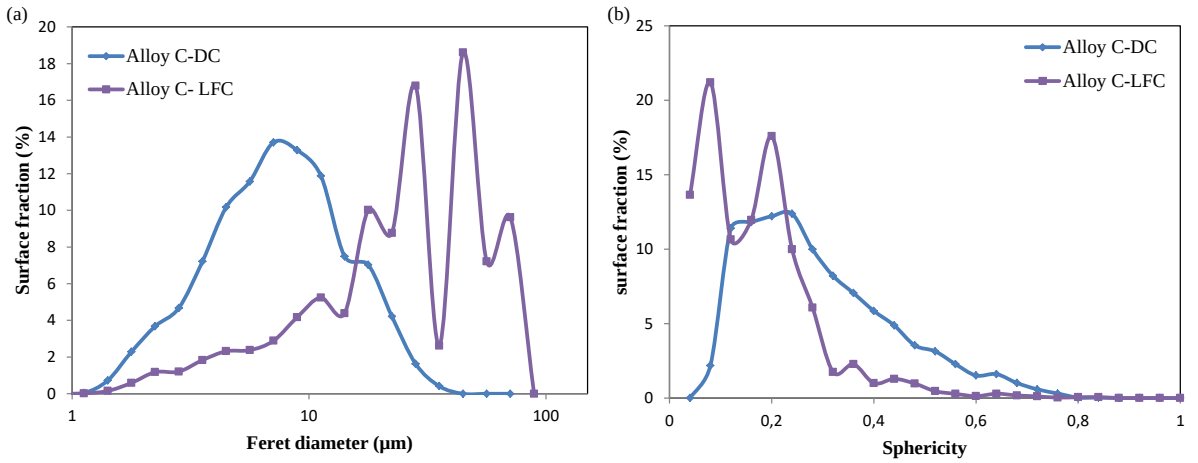

Figure 12 Distributions of Al_2Cu as functions of Feret diameter (a) and sphericity (b) in DC and LFC for alloy C

3.2 Mechanical properties

The mechanical properties, such as hardness, UTS, YS and elongation (%El) values obtained in the present study were analyzed with respect to the different microstructure involved, viz. SDAS, amount, size of eutectic Si, iron Intermetallic compounds, and porosity. The relationship between the microstructure and mechanical properties for the studied alloys will be discussed in the following sections.

3.2.1 Hardness test

The hardness trend observed in the different alloys shows an opposite behavior to SDAS value (Table 6) when comparing DC to LFC alloy C at an almost constant area fraction of iron intermetallic. The Vickers hardness of alloy C decreases from 80.8HV to 63.5HV when the SDAS increases from 18.4µm (DC) to 76.4µm (LFC); this result proves that the evolution of hardness also depends on the SDAS of alloys. In agreement with the results from Sanna et al. [24], Sofyan et al. [41] and Krupiński et al. [42], the hardness decreases with an increase in the size of SDAS.

Table 6 Vickers hardness, area fraction of iron-intermetallic and DAS measured from investigated alloys

Alloy	Casting process	Average Vickers hardness (HV/30)	Area fraction of iron-intermetallic (%)	Mean SDAS (µm)
A	DC	73.7	0.16	20.8
B	DC	74.9	0.22	19.5
C	DC	80.8	1.81	18.4
	LFC	63.5	2.32	76.4
D	DC	83.8	2.48	17.0

To investigate the influence of Sr, Fe and Mn content on the variation in hardness, Vickers hardness measurements for each alloy are reported in Table 6. Sr addition from 47ppm (alloy A) to 130ppm (alloy B) has no obvious effect on the hardness. However, comparison of the alloys A, B and C shows that the hardness increases from 85.3HB (alloy B) to 95.1HB (alloy D) when the iron content increases from 0.1 wt. % to 0.8 wt. %. Besides the alloy D, where the Fe level was highest (0.8%), shows the highest hardness value. This hardness increase is in agreement with Ref. [11, 17], where it is reported that the increase of Fe content increases the hardness of Al-Si alloys as the Fe-intermetallic surface fractions increase. The hardness strongly depends on the composition and fraction of phases in the material. According to Seifeddine et al. [43], the hardness of intermetallic compounds obtained from nanoindentation measurements, i.e. β-Al_5FeSi-needle (11.5 GPa) and α-$Al_{15}(Fe, Mn)_3Si_2$-script phase (14.8 GPa), is larger than that of Al matrix (2.1 GPa). Thus, the almost linear hardness increase with the amount of hard phase reported in Table 6 can be expected for a given SDAS value.

3.2.2 Tensile test

The tensile properties (i.e., ultimate tensile strength, Young modulus, yield strength and elongation) at room temperature are shown in Table 7.

- **The effect of Sr**

By comparing alloy A with B, the Sr content increase from 47ppm to 130ppm has no obvious influence on the UTS and YS. Thus slightly different morphology of eutectic Si resulting from a different Sr

content has a negligible effect on the mechanical properties. The slight decrease of plastic elongation may be due to the increased pore volume fraction [10]. In addition, the Young's modulus depends on the volume fraction of the alloy components (such as Al matrix and hard inclusions) [44] and has no obvious reason to vary with Sr. Besides, as shown in Table 7, the variation of Young's modulus with Sr is within the standard deviation.

Table 7 Tensile properties of studied alloys

Alloy	Casting process	Young modulus [GPa]	Yield Strength [MPa]	Ultimate Tensile Strength [MPa]	Plastic Elongation [%]
A	DC	75.2±4.5	81	256±3	3.8±0.3
B	DC	71.2±3.8	83	258±4	3.2±0.5
C	DC	77.6±6.0	88	254±10	2.1±0.2
	LFC	67.5±1.2	78	180±3	0.29±0.02
D	DC	80.4±5.1	93	239±3	1.3±0.1

- **The effect of Fe and Mn**

The effect of Fe content on the mechanical properties of the DC AlSi7Cu3 alloys is shown in Figure 13. A slight increase in the yield strength, a slight decrease in the UTS and a significant decrease in the elongation is observed when increasing the Fe-Mn content. The elongation to failure decreases due to the increased volume fraction of iron-intermetallics especially the needle-like β-phase [2]. As mentioned previously, the Fe-containing intermetallics particles are more easily fractured under tensile load than the aluminium matrix or the fine silicon particles [45]. As reported by Wang et al. [46], the cracking of Fe-rich compounds tends to account for most of the damage when the Si particles are small. On the other hand, due to the very low pore volume fraction (i.e. 0.03% to 0.06%) in the DC alloys, the effect of pore on elongation is negligible compared to the effect of Fe-containing intermetallics. In addition, Fe can slightly increase the yield strength of Al–Si alloys as reported by Ji et al. [47], and this is usually accompanied by an increase in hardness. The experimental results have confirmed that the amount of Fe-rich intermetallics significantly affect the mechanical properties of the Al–Si–Cu alloys.

Table 6 and Table 7 show that the Young's modulus increased from 71.2 GPa to 80.4 GPa when the surface fraction of iron-intermetallics increased from 0.22% to 2.48%, i.e. for the alloys B and D. This increase of Young modulus with Fe content is mainly due to the hardness and rigidity of iron-intermetallics, which is higher than that of Al matrix [13].

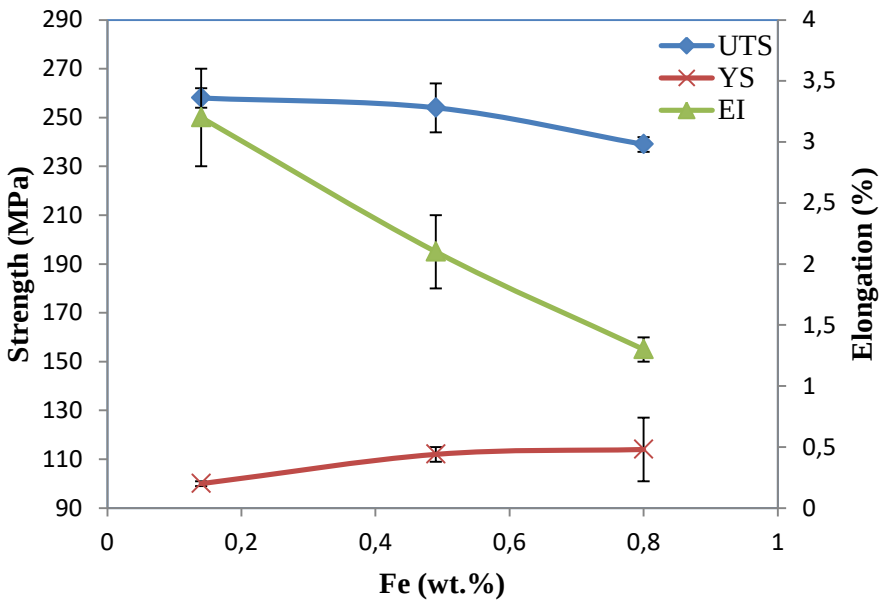

Figure 13 The effect of Fe content on the mechanical properties of the DC AlSi7Cu3 alloys (YS: yield strength; UTS: ultimate tensile strength; El: elongation).

- **The effect of casting process**

The mechanical properties also depend on the casting process. As shown in Table 7, the lower Young's modulus and yield strength of LFC alloy as compared to DC alloy can be explained by the pore volume fraction that is higher in LFC alloy than in DC alloy [48]. Besides, Seifeddine et al. [49] reported that the dendrites are likely to get enriched with Si at a rapidly cooling rate; the higher Si induces a higher strength of the Al matrix in DC alloy.

The average ultimate tensile strength (UTS) has significantly decreased from 254MPa for DC alloy to 180 MPa for LFC alloy, this might be due to the lower SDAS in DC alloy [50]. However, the plastic elongation of LFC alloy is severely reduced compared with DC alloy with a plastic elongation that decreased from 2.1% for the DC alloy to 0.15% for the LFC. The decreased elongation can be attributed to the more numerous and larger pores and coarser microstructures in terms of larger SDAS [51], plate-like eutectic Si particles, iron-intermetallics in LFC alloy compared to DC alloy. These coarser flakes of eutectic Si particles (Figure 7) in LFC alloy promote brittleness. Hafiz et al. [52] reported that the nucleated crack seems to propagate in a brittle manner in the large plate-like eutectic Si particles while Si particles having a fine fibrous morphology fracture in a ductile fashion. Besides, as reported by Ma et al. [10], the β-Al_5FeSi platelet size is also essential to Al-Si alloy ductility and increasing β platelet size from 25 μm to 200 μm causes a significant decrease in elongation (from 14% to 1%). As shown in Table 4, the maximum length of iron-intermetallic increases from 56.3 μm in DC alloy to 245.5 μm in LFC alloy. In addition, the presence of pores facilitates fracture. Large pores, especially shrinkage pores, have an irregular 3D shape, which induces stress concentration, and they are usually responsible for crack initiation during loading [53] as reported by Wang et al. for an A319 LFC alloy [54]. The large shrinkage porosity found in LFC alloy (Figure 2e) may impose this detrimental effect on mechanical properties. Therefore, DC alloys with the refinement of microstructures (i.e. eutectic Si, iron-intermetallics) and fewer defects tend to show higher tensile properties.

4 Conclusion

In the present study, five batches of AlSi7Cu3 alloy with different contents in alloying elements (Sr, Fe and Mn) were obtained by two different casting processes (DC and LFC). Microstructural and mechanical characterizations were performed to relate microstructural features resulting from different metallurgical parameters to mechanical properties. The following main conclusions could be drawn:

1. The size of the dendrites is strongly affected by the cooling rate. However, the chemical composition of the alloys has also some effect on the SDAS, which slightly decreases with the incremental addition of Sr, Fe and Mn.
2. A finer and more fibrous eutectic Si structure can be obtained with an increased Sr content with the drawback that the Sr addition can introduce more pores in the DC alloy. However, no change of the tensile properties with the Sr content increase from 47ppm to 130ppm was noticed.
3. The morphology and surface fraction of iron-intermetallic are influenced by the Fe and Mn content: the amount of Fe-intermetallics (α-$Al_{15}(Fe,Mn)_3Si_2$ and β-Al_5FeSi phase) increases with an increase in the Fe-Mn level while the ratio of α and β phases increased with the increase of Mn/Fe. In addition, a slight decrease of pore volume fraction is observed with an increase in the Fe and Mn content in some extent.
4. Iron has a detrimental effect on the UTS and above all on ductility in terms of the amount of β-Al_5FeSi phase. However, Fe addition increases YS in the alloys studied, i.e. the presence of iron can harden the alloy to some extent.
5. Mechanical properties of AlSi7Cu3 alloy are highly influenced by casting process by the intermediate of the microstructure. The LFC AlSi7Cu3 alloy shows more casting defects (i.e. larger pores and microshrinkage cavities), a coarser microstructure (i.e. larger SDAS, plate-like eutectic Si particles, needle-like iron-intermetallics) than DC AlSi7Cu3 alloy. DC alloys showed higher UTS, YS and elongation than LFC alloy.

In order to understand the damage mechanisms associated to the different hard inclusions characteristics that result from different Sr, Fe, Mn content and casting process, ongoing studies examine the role of the different hard particles (i.e. eutectic Si, iron-intermetallics and Al_2Cu phases) on the propagation of cracks by *in-situ* tensile tests observation.

Acknowledgement

The authors wish to thank the ANR (Agence Nationale de la Recherche) MatetPro project INDiANA (ANR-12RMNP-0011) for funding the study on Al-Si alloys. The ISIS4D X-Ray CT platform (LML, France) is also acknowledged for microtomographic acquisition.

References

[1] Kaufman JG, Rooy EL. Aluminum alloy castings: properties, processes, and applications: ASM International; 2004.
[2] Seifeddine S, Svensson IL. The influence of Fe and Mn content and cooling rate on the microstructure and mechanical properties of A380-die casting alloys. Metallurgical Science and Tecnology. 2013;27.
[3] Albonetti R. Porosity and Intermetallic Formation in Lost Foam Casting of 356 Alloy: National Library of Canada= Bibliothèque nationale du Canada; 2001.
[4] Mbuya T, Odera B, Ng'ang'a S, Oduori F. Effective Recycling of Cast Aluminium Alloys for Small Foundries. JOURNAL OF AGRICULTURE, SCIENCE AND TECHNOLOGY. 2011;12.
[5] Fabrizi A, Ferraro S, Timelli G. The influence of Sr, Mg and Cu addition on the microstructural properties of a secondary AlSi9Cu3 (Fe) die casting alloy. Materials characterization. 2013;85:13-25.

[6] Dahle AK, Nogita K, McDonald SD, Dinnis C, Lu L. Eutectic modification and microstructure development in Al–Si Alloys. Materials Science and Engineering: A. 2005;413–414:243-8.
[7] Dinnis C, Dahle A, Taylor J, Otte M. The influence of strontium on porosity formation in Al-Si alloys. Metallurgical and materials transactions A. 2004;35:3531-41.
[8] Hurtalová L, Tillová E, Chalupová M, Ďuriníková E. Effect of chemical composition of secondary Al–Si cast alloy on intermetallic phases. Mach Technol Mater. 2012;6:11-4.
[9] Yi JZ, Gao YX, Lee PD, Lindley TC. Effect of Fe-content on fatigue crack initiation and propagation in a cast aluminum–silicon alloy (A356–T6). Materials Science and Engineering: A. 2004;386:396-407.
[10] Ma Z, Samuel AM, Samuel FH, Doty HW, Valtierra S. A study of tensile properties in Al–Si–Cu and Al–Si–Mg alloys: Effect of β-iron intermetallics and porosity. Materials Science and Engineering: A. 2008;490:36-51.
[11] Tash M, Samuel F, Mucciardi F, Doty H. Effect of metallurgical parameters on the hardness and microstructural characterization of as-cast and heat-treated 356 and 319 aluminum alloys. Materials Science and Engineering: A. 2007;443:185-201.
[12] Narayanan LA, Samuel F, Gruzleski J. Crystallization behavior of iron-containing intermetallic compounds in 319 aluminum alloy. Metallurgical and Materials Transactions A. 1994;25:1761-73.
[13] Seifeddine S, Johansson S, Svensson IL. The influence of cooling rate and manganese content on the β-Al5FeSi phase formation and mechanical properties of Al–Si-based alloys. Materials Science and Engineering: A. 2008;490:385-90.
[14] Moustafa MA. Effect of iron content on the formation of β-Al5FeSi and porosity in Al–Si eutectic alloys. Journal of Materials Processing Technology. 2009;209:605-10.
[15] Roy N, Samuel A, Samuel F. Porosity formation in AI-9 Wt pct Si-3 Wt pct Cu alloy systems: Metallographic observations. Metallurgical and Materials transactions A. 1996;27:415-29.
[16] Taylor J, Schaffer G, StJohn D. The role of iron in the formation of porosity in Al-Si-Cu-based casting alloys: Part I. Initial experimental observations. Metallurgical and Materials transactions A. 1999;30:1643-50.
[17] Moustafa M. Effect of iron content on the formation of β-Al 5 FeSi and porosity in Al–Si eutectic alloys. Journal of Materials processing technology. 2009;209:605-10.
[18] Dinnis CM, Taylor JA, Dahle AK. Iron-related porosity in Al–Si–(Cu) foundry alloys. Materials Science and Engineering: A. 2006;425:286-96.
[19] Dezecot S, Buffiere J-Y, Koster A, Maurel V, Szmytka F, Charkaluk E, et al. In situ 3D characterization of high temperature fatigue damage mechanisms in a cast aluminum alloy using synchrotron X-ray tomography. Scripta Materialia. 2016;113:254-8.
[20] Standard A. E155. Standard Reference Radiographs for Inspection of Aluminum and Magnesium Castings. 2010.
[21] Ruxanda R, Stefanescu DM. Graphite shape characterisation in cast iron-from visual estimation to fractal dimension. International Journal of Cast Metals Research. 2002;14:207-16.
[22] ISO E. 6892-1: 2009. Metallic materials–tensile testing–Part. 2009;1:6892-1.
[23] Albonetti R. POROSITY AND INTERMETALLIC FORMATION IN LOST FOAM CASTING OF 356 ALLOY.pdf. 2000.
[24] Sanna F, Fabrizi A, Ferraro S, Timelli G, Ferro P, Bonollo F. Multiscale characterisation of AlSi9Cu3 (Fe) die casting alloys after Cu, Mg, Zn and Sr addition. La Metallurgia Italiana. 2013.
[25] Sivarupan T, Caceres CH, Taylor JA. Alloy Composition and Dendrite Arm Spacing in Al-Si-Cu-Mg-Fe Alloys. Metallurgical and Materials Transactions A. 2013;44:4071-80.
[26] Emadi D, Gruzleski J, Toguri J. The effect of Na and Sr modification on surface tension and volumetric shrinkage of A356 alloy and their influence on porosity formation. Metallurgical Transactions B. 1993;24:1055-63.
[27] Liu L, Samuel A, Samuel F, Doty H, Valtierra S. Influence of oxides on porosity formation in Sr-treated Al-Si casting alloys. Journal of materials science. 2003;38:1255-67.
[28] Argo D, Gruzleski J. Porosity in modified aluminum alloy castings. AFS Transactions. 1988;96:65-74.

[29] Dash M, Makhlouf M. Effect of key alloying elements on the feeding characteristics of aluminum–silicon casting alloys. Journal of Light Metals. 2001;1:251-65.
[30] Puncreobutr C, Lee PD, Hamilton RW, Phillion AB. Quantitative 3D Characterization of Solidification Structure and Defect Evolution in Al Alloys. JOM. 2012;64:89-95.
[31] Dinnis C, Taylor J, Dahle A. Porosity formation and eutectic growth in Al-Si-Cu-Mg alloys containing iron and manganese. Materials Forum-Aluminium Alloys Their Physical and Mechanical Properties: The Institute of Materials Engineering Australasia Ltd; 2004. p. 1016-21.
[32] Emadi D, Gruzleski JE. Combating Al-Si porosity: the strontium/hydrogen myth. Modern casting. 1995;85:46-7.
[33] Caceres C, Selling B. Casting defects and the tensile properties of an AlSiMg alloy. Materials Science and Engineering: A. 1996;220:109-16.
[34] Hegde S, Prabhu KN. Modification of eutectic silicon in Al–Si alloys. Journal of materials science. 2008;43:3009-27.
[35] Haque MM. Effects of strontium on the structure and properties of aluminium-silicon alloys. Journal of Materials Processing Technology. 1995;55:193-8.
[36] Kosa A, Gacsi Z, Dúl J. Effects of strontium on the microstructure of Al–Si casting alloys. Materials Science and Engineering. 2012;37:43-50.
[37] Lu L, Dahle A. Iron-rich intermetallic phases and their role in casting defect formation in hypoeutectic Al− Si alloys. Metallurgical and Materials Transactions A. 2005;36:819-35.
[38] Ceschini L, Boromei I, Morri A, Seifeddine S, Svensson IL. Microstructure, tensile and fatigue properties of the Al–10% Si–2% Cu alloy with different Fe and Mn content cast under controlled conditions. Journal of Materials Processing Technology. 2009;209:5669-79.
[39] Li Z, Samuel A, Samuel F, Ravindran C, Valtierra S. Effect of alloying elements on the segregation and dissolution of CuAl2 phase in Al-Si-Cu 319 alloys. Journal of materials science. 2003;38:1203-18.
[40] Labisz K, Krupiński M, Dobrzański L. Phases morphology and distribution of the Al-Si-Cu alloy. Journal of Achievements in Materials and Manufacturing Engineering. 2009;37:309-16.
[41] Sofyan BT, Kharistal DJ, Trijati L, Purba K, Susanto RE. Grain refinement of AA333 aluminium cast alloy by Al–Ti granulated flux. Materials & Design. 2010;31:S36-S43.
[42] Krupiński M, Labisz K, Dobrzański L, Rdzawski Z. Derivative thermo-analysis application to assess the cooling rate influence on the microstructure of Al-Si alloy cast. journal of Achievements in Materials and Manufacturing Engineering. 2010;38:115-22.
[43] Seifeddine S, Johansson S, Svensson IL. The influence of cooling rate and manganese content on the β-Al 5 FeSi phase formation and mechanical properties of Al–Si-based alloys. Materials Science and Engineering: A. 2008;490:385-90.
[44] Lasagni F, Degischer HP. Enhanced Young's Modulus of Al-Si Alloys and Reinforced Matrices by Co-continuous Structures. Journal of composite materials. 2010;44:739-55.
[45] Taylor JA. The effect of iron in Al-Si casting alloys. 35th Australian foundry institute national conference, Adelaide, South Australia2004. p. 148-57.
[46] Wang L, Apelian D, Makhlouf M. Tensile properties of aluminum die-casting alloys. Proceedings of the 19th International Die Casting Congress, Minneapolis, NADCA, Rosemont, IL1997. p. 179-89.
[47] Ji S, Yang W, Gao F, Watson D, Fan Z. Effect of iron on the microstructure and mechanical property of Al–Mg–Si–Mn and Al–Mg–Si diecast alloys. Materials Science and Engineering: A. 2013;564:130-9.
[48] Mugica GW, Tovio DO, Cuyas JC, González AC. Effect of porosity on the tensile properties of low ductility aluminum alloys. Materials Research. 2004;7:221-9.
[49] Seifeddine S, Svensson IL. Prediction of mechanical properties of cast aluminium components at various iron contents. Materials & Design. 2010;31, Supplement 1:S6-S12.
[50] Ceschini L, Morri A, Morri A, Gamberini A, Messieri S. Correlation between ultimate tensile strength and solidification microstructure for the sand cast A357 aluminium alloy. Materials & Design. 2009;30:4525-31.
[51] Li Z, Samuel A, Samuel F, Ravindran C, Valtierra S, Doty H. Parameters controlling the performance of AA319-type alloys: Part I. Tensile properties. Materials Science and Engineering: A. 2004;367:96-110.

[52] HAFIZ M, KOBAYASHI T. Mechanical properties of modified and nonmodified eutectic Al-Si alloys. Keikinzoku. 1994;44:28-34.
[53] Savelli S, Buffière JY, Fougeres R. Pore characterization in a model cast aluminum alloy and its quantitative relation to fatigue life studied by synchrotron X-ray microtomography. Materials science forum: Trans Tech Publ; 2000. p. 197-202.

[54] L. Wang, N. Limodin, A. El Bartali, J.-F. Witz, R. Seghir, J.-Y. Buffiere, E. Charkaluk, Influence of pores on crack initiation in monotonic tensile and cyclic loadings in lost foam casting A319 alloy by using 3D in-situ analysis, Materials Science and Engineering: A. 673 (2016) 362–372. doi:10.1016/j.msea.2016.07.036.